Suplemento de la Revista Mexicana de Física **1** (3) 49–54 JULY–AUGUST 2020

Optical biosensor for biogenic amines detection used a porous silicon matrix

J.A. Contreras[a], F. Severiano[b], V. L. Gayou[a], H. Martínez Gutiérrez[c], and R. Delgado Macuil[a,*]
[a]*Instituto Politécnico Nacional, Centro de Investigación en Biotecnología Aplicada Unidad Tlaxcala, 90700 Carretera Santa Inés Tecuexcomac Km 1.5, Ex-Hacienda San Juan Molino.*
[*]*e-mail: rdelgadom@ipn.mx*
[b]*Consejo Nacional de Ciencia y Tecnología, Av. Insurgentes Sur 1582, Col. Crédito Constructor, Del. Benito Juárez, 03940, Cd. de México.*
[c]*Instituto Politécnico Nacional, Centro de Nanociencias, y Micro y Nanotecnologías, Calle Luis Enrique Erro s/n, Unidad Profesional Adolfo López Mateos, Col. Zacatenco, 07738 Cd. de México.*

Received 9 September 2019; accepted 3 December 2019

The content of biogenic amines has been studied due to the toxicity of these compounds in humans when are consumed exogenously and is used as an indicator of quality in the food industry. The manly method for its determination is high-performance liquid chromatography. However, it requires a long time for analysis. An alternative method is the use of biosensors. Porous silicon is a material with the potential to be applied in bio-delivery carriers and biosensors. Once these substrates were obtained, they were used for the construction of a biosensor capable of detecting biogenic amines using diamine oxidase enzyme as an element of biological recognition and is binding using the self-assembled monolayers method. The correlation between scanning electron microscopy, X-ray dispersive energy spectroscopy, and Fourier Transform infrared spectroscopy analysis, showed the correct construction of the biosensor and the detection of biogenic amines by interaction with the enzyme. Finally, with the built biosensor it was possible to detect putrescine, cadaverine and spermidine; three important biogenic amines found in food.

Keywords: Biogenic amine; Biosensor; Self-assembled monolayers; Porous silicon.

PACS: 07.07.Df; 82.80.Gk; 81.05.Rm; 68.37.Hk; 64.75.Yz; 82.80.Ej

1. Introduction

Biogenic amines (BA) are nitrogen compounds with low molecular weight and there has been the replacement of some of the hydrogens by alkyl groups. They can be classified into two large groups [1]: the endogenous ones that are synthesized in different tissues of the superior organisms and the exogenous ones that are ingested in diet, appearing during the process or storage of the food by action of the microorganisms. They are produced by microbial decarboxylation through their amino acids (aa) precursors and they can also be produced by amination or transamination of aldehydes and ketones [2]. On the other hand, the consumption of BA in high concentrations can have harmful effects and cause certain symptoms such as headaches, hypo and hypertension, nausea, heart palpitation, renal intoxication, in more severe cases cerebral hemorrhage, and even death [3]. In addition to their toxicological effects, BA, such as: related to food hygiene, their presence in high concentrations may be indicative of the use of poor quality raw materials, contamination and inappropriate conditions during food processing and storage [4]. However, there are mechanisms that prevent the formation of BA; they are: temperature control, use of good quality materials, good manufacturing practices, use of starter cultures, presence of amine oxidants, and the maintenance of high hydrostatic pressure [5]. The toxicity of BA will depend on factors associated on the food (qualitative and quantitative) and also with the factors associated with the consumer (susceptibility and health status) [6,7]. At present, regulations have been established only for the intake of histamine, but limits have been set for other BA, including putrescine and cadaverine. The allowed maximum residue level of histamine in food, according European Economic Community (EEC) regulations, is 100 mg/kg [8]. The technique commonly used for the determination of BA in food is high-performance liquid chromatography due to its high resolution and sensitivity [9], but this technique is time-consuming and requires special instrumentation [10]. The application of biosensors for BA analyses is a good alternative to the traditional method, due to their specificity, short analysis time, simplicity and possibility to be used outside in an organized laboratory.

Catalytic biosensors can use enzymes, antibodies, tissues, cell receptors, microorganisms, etc. as a biological recognition element (BRE). Interacting the BRE with the analyte will result in a measurable change in the property of the solution, such as the depletion of a reagent or the formation of a product, without the catalyst being consumed, with enzymes being the most used elements for the manufacture of these biosensors due to their low cost, availability in the market and easy handling [11]. The biosensors include those of the optical type, which use the measurement of the variation of the optical properties, their success is mainly based on two factors: the immobilization of enzymes in solid substrates to improve the shelf life, and storage time of biosensors, improving sensitivity and detection limit. The second factor is the use of optical transducers; the affinity of the biosensor depends on the selectivity of the biological component and the transducer sensitivity [12].

Porous silicon (PS) and silicon nanocrystals have properties that are particularly interesting and suitable for applications in the biological sensor industry. PS-based biosensors offer increased sensitivity, reduced energy demand, are of low cost, biocompatible and have a very large surface area. In addition to presenting electroluminescence and being biodegradable, it shows a non-toxic behavior when used in humans [13]. To improve the selectivity of the biosensor through specific interactions some researchers have proposed to modify, chemically or physically, the surface of the silicon filaments in the pores of PS [14]. It is generally proposed to generate covalent bonds between the surface of the PS and the biomolecule, which recognizes a particular analyte [15]. Such recognition occurs when the analyte interacts with the previously modified sensor with an organic molecule that provides specificity.

To provide specificity will be used amine oxidase. This biological element is a Cu^{+2} or Copper-containing Amine Oxidases (CAO) dependent enzyme that catalyzes the oxidative deamination of different amines to form the corresponding aldehydes, producing equal amounts of ammonium and hydrogen peroxide. It has a classic ping-pong type catalysis mechanism composed of two reactions, the first one where the enzyme is reduced by the substrate Eq. (1) and the second, which consists of the re-oxidation of the enzyme by molecular oxygen Eq. (2) [16].

$$E_{ox} + R - CH_2 - NH_3 \rightarrow E_{red} - NH_3 + R - CHO \quad (1)$$

$$E_{red} - NH_3 + O_2 + H_2O \rightarrow E_{ox} + NH_4 + H_2O_2 \quad (2)$$

PS is obtained by chemical etching using chloroauric acid ($HAuCl_4$) in the electrolyte, considering a simple and alternative method to conventional methods (cathodic spraying, chemical vapor deposition, electrodeposition, electrolysis) [17]. This technique is based on localized oxidation, reduction of reactions under open circuit and dissolution of silicon (Si) in hydrofluoric acid (HF) while metal (usually a noble metal) catalytically improves the process of engraving [18]. As a result, the metal is deposited as nanoparticles in the Si substrate where the pores are generated. Obtaining PS structures of a wide range of sizes between 5 nm and bigger than 1 μm. In addition, it allows adjusting the physical properties of the PS (thickness, pore diameter and doping level). The thickness is controlled through the engraving time; the pore diameter is controlled by the electrolyte used; and the level of doping is controlled by the amount of metal salt supplied [19].

Proteins can be covalently coupled onto surfaces using the two-step coupling protocol with 1-ethyl-3-3 [3dimethyl] (EDC) which is a water-soluble carbodiimide. The reaction forms an intermediate product (O-acylisourea) that reacts rapidly with primary amines to form a stable amide bond. This intermediate product is unstable and easily hydrolyzed with water; to avoid this rapid hydrolysis, N-hydroxysuccinimide is added to form a more stable NHS-ester product that reacts slowly with the primary silane amines and forms a stable amide bond [20]. According to the aforementioned, the main objective of this work is to build an optical biosensor for the determination of BA. The idea of using the enzyme diamine oxidase (DAO) is due to the selectivity with the analyte of interest. In this way, the use of gold nanoparticles (AuNPs) in the structure of PS improves the sensitivity of the biosensor.

2. Experimental Methods

It was used P-type silicon wafer boron-doped with a resistivity of 5-10 Ω/cm and oriented according to the crystalline direction (100) to obtain PS with AuNPs. The method of chemical etching assisted with metal salt was used to obtain the substrates [21]. The anodization process was carried out in an electrochemical cell made of teflon and as a cathode was used a tungsten mesh, which is similar in size to the wafer area in contact with the electrolyte. The substrate acts as an anode by being in contact with an iron plate on its external face. The electrolyte was composed by a mixture of hydrofluoric acid (HF, Merck 40% by volume), ethanol (Alfa Aesar 99.98% by volume) and chloroauric acid (HAuCl4 trace metals basis, diluted at 30 wt % in HCl (Sigma Aldrich)) and at a constant current density of 2 mA/cm^2. The metal salt was prepared at a ratio of 0.75 mM, and then incorporated in the electrolyte. The volume ratios used in the electrolyte were 1/2/1, HF/ethanol/$HAuCl_4$ respectively, and the etching time was 1 hour.

2.1. PSAuNPs silanization

The internal Surface of the PS matrix is hydrogen-terminal after the etching, which allows immobilizing biomolecules on the porous surface, so is not necessary to go through an activation process [22]. The silanization of PSAuNPs substrates was carried out in a solution of 3-aminopropyltrimethoxysilane (3-APTMS) in preheated toluene between 90-100°C for 1 hour. The solution was prepared at 2% of 3-APTMS in volume. Subsequently, the substrates were removed from the solution and rinsed with toluene and dried in an oven at 100°C for 1 hour.

2.2. Inmovilization process

DAO immobilization was carried out (from Pea seed, activity 91.1 IU/mL from DiaMaze) on silanized PSAuNPs substrates by activation of carboxyl groups of the enzyme by means of EDC/NHS [23]. This method is known as EDC/NHS coupling and results in robust amide bond formation. EDC/NHS chemistry has been employed as a covalent attachment methodology for the immobilization of proteins and as a method for the preparation of substrates. This method is known as EDC/NHS coupling and results in robust amide bond formation. The mixture consisted of 6.5/18.3 mg/mL of EDC/NHS, directly in the liquid DAO (1 mL) and was agitated for 20 min at 350 rpm and filtered (using a 0.45 μm

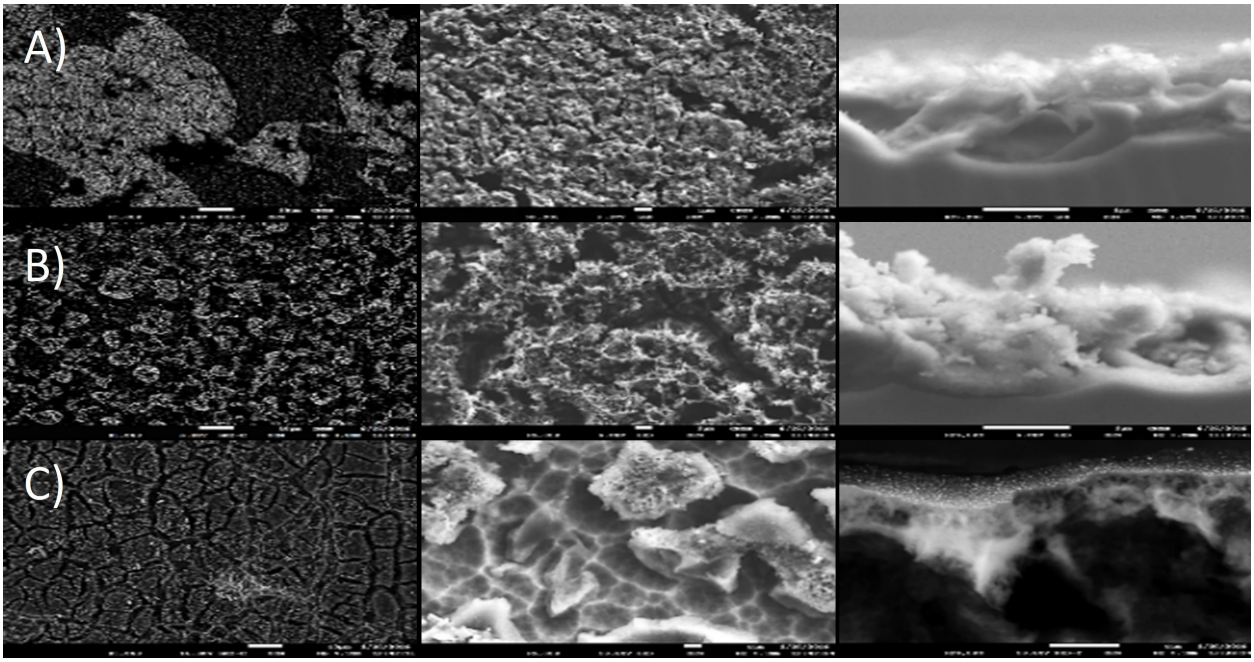

FIGURE 1. SEM micrographs of the assembly stages of the 1000X and 5000X biosensor of the top view, and 5000X of the cross-section of the material respectively from left to right. A) PSAuNPs B) Silanized PSAuNPs. C) DAO immobilized on the substrate surface.

Nylon membrane). Finally, 300 μL of the mixture were placed on the surface of the substrates and left for a 1 hour at room temperature.

2.3. Biosensor characterization

The biosensor was characterized by Fourier-transform infrared spectroscopy (FTIR) using the transmission mode at each step of assembly. FTIR spectra were collected with a spectrometer Bruker Vertex 70 and each spectrum was the average of 120 repetitions. SEM images were obtained using a high-resolution field emission scanning electron microscope JEOL JSM-7800F to study the morphology and cross-section of the porous silicon layer (PSL) in the sample. The chemical composition was obtained by an X-ray energy dispersive spectrometer (EDAX AMETEK) coupled at the SEM system.

2.4. BA detection

BA sensing was performed by FTIR in the infrared region (400-4000 cm^{-1}) using attenuated total reflectance mode (ATR). The process consisted of detecting ammonium, whose characteristic band appears at 1132 cm^{-1}. In this case, the respective BA solutions were prepared at different concentrations (1000, 800, 600, 400, 200, 100 and 50 ppm) in 50 mM of TRIS buffer at pH 7.2 and then 6 μL of the solution was placed in contact with the biosensor. The interaction kinetics was analyzed for 30 minutes, each spectrum was acquired every 30 seconds. Dilution buffer was used as baseline.

3. Results and discussion

3.1. SEM characterization

Figure 1 shows SEM images of the surfaced and cross-sectional images. The images show the morphological changes at each stage of self-assembly. The micrographics of row A, belong to the PS just obtained, it is possible to observe the spongiform morphology with cavities after etching. In addition, AuNPs are observed on the surface like brilliant points. The row B of micrographs belongs to the stage of silanization of PSAuNPs, a thin and homogeneous coverage of 3-APTMS is observed as a charge accumulation on the substrate without structural changes of the material. On the other hand, the images in row C belongs to the immobilization of the DAO through the formation of an amide bond with EDC/NHS. A more homogeneous and continuous surface with a network of pores is observed, maintaining the presence of AuNPs as observed in the cross-section of this stage. The hypothesis is that the EDC/NHS form a uniform coverage for the reception of the DAO and its covalent union. Previously the pore size, thickness and nanoparticle size were characterized (1.5 μm, 4 μm and $\sim$ 20 nm respectively) [19].

3.2. EDX characterization

Figure 2 shows the EDX analysis of each stage self-assembled process, a) shows the freshly prepared PS, this analysis shows the presence of the peak attributed to gold (2.1 KeV). This analysis reinforces the SEM images, that the nanoparticles remain on the surface of the material. In turn, an intense peak related to oxygen (0.5 KeV) is observed.

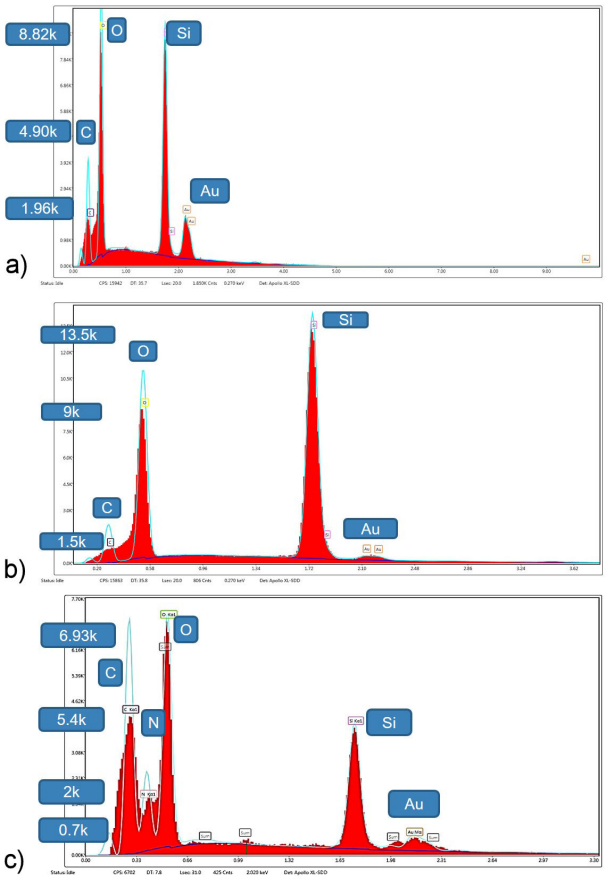

FIGURE 2. SEM EDX analysis. a) EDX spectrum of the freshly prepared PS. b) EDX spectrum of PSAuNPs after the silanization process. c) EDX spectrum of the biosensor assembled in the enzyme immobilization stage.

After the silanization process according to the EDX analysis, no changes are observed in the spectrum obtained. However, the binding of the organosilane to the substrate is confirmed by means of FTIR. In addition, a decrease in peak intensity corresponding to gold in the sample is observed, see Fig. 2b).

Figure 2c) shows the EDX analysis of the biosensor in the immobilization stage, the presence of gold in the sample until this step is possible see it. In this way, the results obtained through SEM are reinforced, where the AuNP remain on the surface of the material after the treatments carried out. In turn, an oxygen-related peak (0.5 KeV) is shown but is less intense than in the previous stages. The presence of the carbon peak in the spectrum is also observed confirming the presence of molecules inserted in the material, such as methylene groups (-CH3) linked in the silanization process or the presence of carbon in carbonyl groups (C=O) of proteins. Otherwise, the presence of nitrogen is confirmed once the enzyme is immobilized in the substrate and reinforced the FTIR analysis.

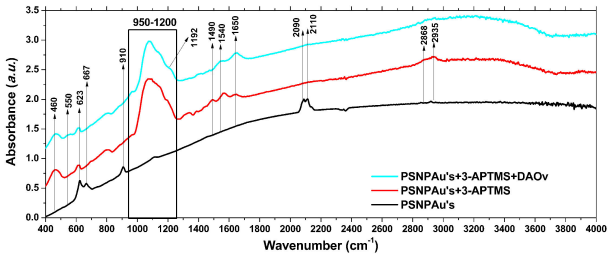

FIGURE 3. FTIR absorption spectra of the biosensor assembly in transmission mode.

3.3. FTIR Characterization

Figure 3 shows all FTIR spectra in the transmission mode of the assembly steps of the biosensor. The black spectrum belongs to the freshly prepared PSAuNPs and shows the characteristic bands of Si-Hx [24]. The bands 623, 667 and 910 cm^{-1} are related to hydride bending. Finally, the bands in 2090 and 2110 cm^{-1} also related to the vibration of hydrides (Si-Hx) [25,24]. The red spectrum was obtained after immersion for 1 hour in 2% of 3-APTMS solution. This compound improves the adsorption of biomolecules to the surface. 3-APTMS are molecules with a small size (0.7-0.8 nm) so they can easily infiltrate the pores (1.5 μm) of the SPNAu's substrate [26]. Absorption bands associated with silanization is by the presence of different vibrational modes related to NH_2, CH_2 and SiO bonds. The band at 460 cm^{-1} is associated with the vibrations of the Si-OH bond [27,28], the bands at 667 and 910 cm^{-1} are associated with hydride bending (Si-Hx) and the Si-OH bond respectively, which are attenuated after silanizing the substrates. The bands in 1066, 1150 and 1228 cm^{-1} that are observed more intense in the spectrum of silanized PSAuNPs are associated to the Si-O-Si bonds, these vibrations are included in the region between 950 and 1250 cm^{-1} [27,28]. Another important feature to highlight is the 1192 cm^{-1} band related to the balance of the unreacted Si-O-C and Si-O-CH_3 groups during the formation of the silanization monolayer [29]. The bands in 1472 and 2935 cm^{-1} correspond to the methylene groups (-CH2) of the alkyl chain containing the amino functional group (NH2), the presence of this functional group is at 1565 cm^{-1}, this band is very important for the immobilization of biomolecules, because it allows the formation of the amino bond between the surface and the enzyme. The 1648 cm^{-1} band corresponds to the protonation of the amino group when exposed to the environment [30]. The results showed that the process of functionalization was successful. The blue spectrum corresponds to the immobilization stage of the DAO enzyme on the PSAuNPs substrates. The spectral response in the medium IR of the biosensor assembled by amide bond formed by the amino terminal group of the silanization process and the activated carboxyl groups of the enzyme by EDC/NHS. It is possible to observe an attenuation of the bands at 460 and 550 cm^{-1}. The spectral region between 950-1200 cm^{-1} is also attenuated after immobilization. The bands in 1548 and 1650 cm^{-1}

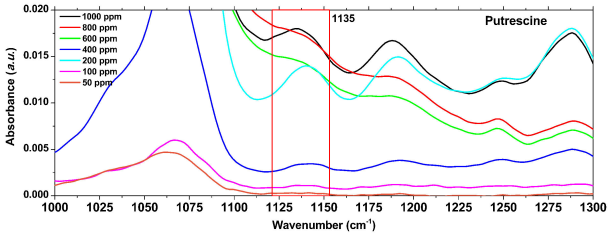

FIGURE 4. Biosensor calibration using putrescine in the region of interest.

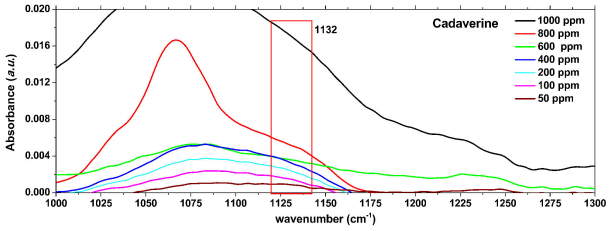

FIGURE 5. Biosensor calibration using cadaverine in the region of interest.

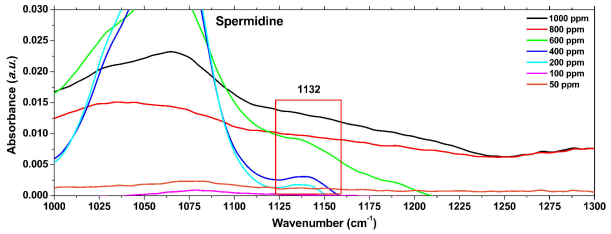

FIGURE 6. Biosensor calibration using spermidine in the region of interest.

are associated with the amide II and amide I of the proteins. Amide II appears in FTIR because of the flexural vibrations of the N-H bonds and stretching of the C-N bond in the plane; and amide I is caused by stretching of the carbonyl group (C=O) and flexion in the plane of the C-N bond. These peaks are related to primary and secondary amines respectively in proteins. These bands can be observed in the spectrum pertaining to immobilization. Through FTIR it was possible confirm if the enzyme has covalently bound to substrate.

3.4. Sensing of BA

The most noticeable changes in the sensing process are due to the interaction between DAO and BA occurred in the CN (1580-1650 cm^{-1}) and NH flexion (1000-1335 cm^{-1}) regions, for our purposes we focus on this last. The spectra were collected every 30 seconds with one interaction per second, for a total of 30 minutes of kinetics (60 spectra). The bands $\sim$ 1070 cm^{-1} and 1132 cm^{-1} increase their intensity over time. The increase in the band $\sim$ 1070 cm^{-1} may be due in part to the production of ammonium. However, may be caused by vibrations of the bonds C-C or C-N of the TRIS buffer solution.

To validate the functioning of the biosensors assembled kinetics were performed using biogenic amines diluted in 50 mM TRIS buffer pH 7. Enzymatic kinetics are shown in Figs. 4, 5 and 6 using putrescine, cadaverine, and spermidine respectively at different concentrations of 1000, 800, 600, 400, 200, 100, 50 ppm. The strategy was to detect one of the DAO reaction products by interacting with the biogenic amine (BA): aminoaldehydes, ammonium and hydrogen peroxide (H_2O_2). The detection of H_2O_2 by FTIR is extremely difficult due to the masking of the water bands, the weak band being 876 cm^{-1} derived from the H-O vibration which that provides information regarding its detection [30], so this spectroscopic technique is not viable for its determination. In addition to the above, during the study of the kinetics of BA with the biosensor, it was not possible to detect the band corresponding to H_2O_2. In the images, the spectra with greater intensity of the kinetics made at a certain concentration are observed. In the case of putrescina, the maximum absorbances for each concentration were 0.0187, 0.0176, 0.0152, 0.00349, 0.0140, 0.00105 and 0.00042 U.A. respectively.

In 2016, an experiment was conducted by Caso, obtaining the spectrum of ammonium hydroxide (NH4OH) found that the broadband corresponding to the flexion within the plane of the NH_4NH bonds covers from 1125-180 cm^{-1} with a maximum in $\sim$ 1100 cm^{-1} [31]. This is very interesting because it is possible to observe a band at 1180 cm^{-1} that as mentioned can be detected ammonium produced from the interaction between the BA and the assembled biosensor. However, this band only is possible detected in the case of putrescine.

Otherwise, biosensor calibration was performed using cadaverine (Fig. 5) with the same concentrations. We observe that there is indeed a linear trend between the absorbance obtained and the concentration used in each sensing. The intensity of the absorbances were 0.0171, 0.00508, 0.00356, 0.00312, 0.00224, 0.00137, and 0.000948 a.u. respectively. In this case, the absorbances were less intense than those obtained with putrescine.

The BA spermidine calibration was carried out with the same concentrations (Fig. 6), we observed that there is indeed a linear trend between the absorbance obtained and the concentration used in each sensing. The intensity were 0.0136, 0.0110, 0.00918, 0.00392, 0.00217, 0.00153 and 0.00128 a.u. respectively. In FTIR the use of AuNPs increases the signal of the samples that are in contact with them through the effect known as SEIRA (surface enhanced infrared absorption) [32]. Although an increase in signal strength may be due to the structure of the porous silicon too.

4. Conclusions

It was possible to obtain samples of PS with the desired pore size with the electrochemical etching method using a metal salt in the electrolyte, suitable for the confinement of biological molecules. Through the analysis spectra of 3-APTMS deposition onto PSAuNPs, we can conclude that 3-APTMS

can be used to functionalize the PS surface in order to attach biomolecules. The characterization of each of the stages was carried out satisfactorily by means of FTIR. DAO enzyme immobilization was achieved through the use of binding agents on the substrate (EDC/NHS). SEM characterization of the biosensor displays morphological differences during the immobilization stages of the DAO. In addition, those results obtained by FTIR were confirmed with the EDX analysis in each of the stages with the incorporation of new elements that make up the biosensor. Thus, it was possible to sense 3 BA of importance in food with the built biosensor.

1. N. Benkerroum, *Compr. Rev. Food Sci. Food Saf.* **15** (2016) 801. https://doi.org/10.1111/1541-4337.12212
2. R. Maijala, and S. Eerola, *Meat Sci.* **35** (1993) 387-395. https://doi.org/10.1016/0309-1740(93)90043-H
3. A. R. Shalaby, S. Kurt, and O. Zorba, *Food Res. Int.* **29** (1996) 675-690. https://doi.org/10.1002/jsfa.4138
4. S. Bover-Cid, S. Schoppen, M. Izquierdo-Pulido, and M. Vidal-Carou, *Meat Sci.* **51** (1999) 305-311. https://doi.org/10.1016/S0309-1740(98)00120-X
5. P. Visciano, M. Schirone, R. Tofalo, and G. Suzzi, *Front. Microbiol.* **3** (2012) 1-10. https://doi.org/10.3389/fmicb.2012.00188
6. F. Gardini *et al*., *Int. J. Food Microbiol.* **64** (2001) 105-117. https://doi.org/10.1016/S0168-1605(00)00445-1
7. C. Ruiz-Capillas, and F. Jiménez-Colmenero, *Crit. Rev. Food. Sci. Nutr.*, **44** (2004) 489-499. https://doi.org/10.1080/10408690490489341
8. J. Karovicova, and Z. Kohajdova, *ChemInform* **36** (2005). https://doi.org/10.1002/chin.200534338
9. P. Hernandez-Orte, A. Peña-Gallego, M. J. Ibarz, J. Cacho, and V. Ferreira, *J. Chromatogr. A*, **1129** (2006) 160-164. https://doi.org/10.1016/j.chroma.2006.06.111
10. M. L. Latorre-Moratalla, S. Bover-Cid, and M. C. Vidal-Carou, *Meat Sci.* **85** (2010) 537-541. https://doi.org/10.1016/j.meatsci.2010.03.002
11. A. S. Hernández Cázares, *Control de calidad y seguridad de la carne y productos cárnicos curados mediante el uso de sensores enzimáticos* **253** (2010).
12. M. M. F. Choi, *Microchim. Acta* **148** (2004) 107-132. https://doi.org/10.1007/s00604-004-0273-8
13. L. C. Lasave, G. I. Priano, R. R. Koropecki, F. Battaglini, and R. D. Arce, *Revista Fabicib*, **14** (2010) 70-83.
14. S.C. Buswell, V.A. Wright, J.M. Buriak, V. Van, and S. Evoy, *Opt. Express* **16** (2008) 15949.
15. K. P. S. Dancil, D. P. Greiner, and M. J. Sailor, *J. Am. Chem. Soc.* **121** (1999) 7925. https://doi.org/10.1021/ja991421n
16. R. Prabhakar, and P. E. M. Siegbahn, *J. Phys. Chem. B* **105** (2001) 4400. https://doi.org/10.1021/jp003343s
17. F. Severiano, *et al*., *Appl. Phys. A* **123** (2017). https://doi.org/10.1007/s00339-016-0718-z
18. T. Qiu, X. L. Wu, G. G. Siu, and P. K. Chu, *Appl. Phys. Lett.* **87** (2005) 1-3. https://doi.org/10.1063/1.2138360
19. Severiano *et al*., *J. Nanosci. Nanotechnol.* **18** (2019) 3604. https://doi.org/10.1166/jnn.2019.16094
20. S. K. Vashist, *Diagnostics*, **2** (2012) 23-33. https://doi.org/10.3390/diagnostics2030023
21. F. Severianoa *et al*., *Frontera Biotecnologica* (2017).
22. H. Li, A. Fu, D. Xu, G. Guo, L. Gui, and Y. Tang, *Langmuir* **18** (2002) 3198.
23. J. A. O. Mendoza, *Determinación de aminas Biogenas por métodos espectroscópicos* (2015). Tesis de Maestria. Instituto Politécnico Nacional. https://doi.org/10.1109/CCECE.2014.6901098
24. Y. Ogata, H. Niki, T. Sakka, and M. Iwasaki, *J. Electrochem. Soc.* **142** (1995) 195. https://doi.org/10.1149/1.2043865
25. P. Gupta, A. C. Dillon, A. S. Bracker, and S. M. George, *Surf. Sci.* **245** (1991) 360. https://doi.org/10.1080/00958972.2013.770846
26. M. Baranowska *et al*., *J. Colloid Interface Sci.* **452** (2015) 180-189. https://doi.org/10.1016/j.jcis.2015.04.022
27. K. T. Queeney *et al*., *Appl. Phys. Lett.* **87** (2000) 1322-1330. https://doi.org/10.1063/1.372017
28. K. T. Queeney, N. Herbots, J. M. Shaw, V. Atluri, and Y. J. Chabal, *Applied Physics Letters* **84** (2004) 493-495. https://doi.org/10.1063/1.1644030
29. J. Kim, P. Seidler, C. Fill, and L. S. Wan, *Surf. Sci.* **602** (2008) 3323-3330. https://doi.org/10.1016/j.susc.2008.09.001
30. J. S. Duque, *Resonancia del plasmon de superficie en nanoparticulas metalicas sintetizadas por ablación laser* (2017).
31. L. Caso, (2016). *Desarrollo de un método de determinación de aminas biógenas en Tilapia por espectroscopias UV/Vis e Infrarrojo*. (Tesis doctoral). Centro de Investigación en Biotecnología Aplicada del IPN, Tlaxcala, México.
32. D. Enders, and A. Pucci, *Appl. Phys. Lett.* **88** (2006) 184104. https://doi.org/10.1063/1.220188